Numerical study of weldability of dissymetric assembly during resistance spot welding

J. Queval[1], A. Ollivier[1], E. Geslain[1], P. Rogeon[1], T. Pierre[1], C. Pouvreau[1], L. Cretteur[2], S. Marie[3]

1 Université Bretagne Sud, IRDL, CNRS FRE 3744, Lorient, France
philippe.rogeon@univ-ubs.fr
2 ArcelorMittal Global R&D, Montataire, France
laurent.cretteur@arcelormittal.com
3 Transvalor S.A., Sophia-Antipolis, France
stephane.marie@transvalor.com

Abstract :

In automotive industry, to simultaneously impact safety and light weighting for reducing energy consumption, new families of high strength steel have been introduced in the design of body in white. Some combinations of dissimilar sheets, including a very thin sheet, cause weldability problems and difficulties to the optimization of the process parameters setting. This work aims at the improvement of the weldability of a dissymmetric combination of three dissimilar sheets: a very thin (0.57mm) zinc coated low carbon steel sheet, a thick (1.47mm) zinc coated advanced high strength steel sheet, and a thick (1.2mm) aluminium-silicium coated press hardened sheet. A numerical axisymmetric 2D Electro-Thermo-Mechanical model developed with the software FORGE® is used to improve the knowledge about the mechanisms which influence the nugget formation and growth, and its penetration inside the cover thin sheet. The model is consistent with several experimental observations (nugget size, contact radii, dynamic resistance) issued from welding tests. The numerical results show that the initial heating is done at the interfaces with the aluminized sheet, opposite the very thin sheet. The lack of penetration of the nugget into the thin sheet is a consequence of the overheating at the interfaces with the aluminized sheet and the uncontrolled growth of the nugget.

Keywords : resistance spot welding / interface / numerical modeling / contact resistance / physics coupling

1 Introduction

In the automotive industry, lightweighting of vehicles is one of the main way to reduce energy consumption. ArcelorMittal, world leader in the production of steels works to develop new high strength grades to meet the same specifications with thinner steel sheets and ensure safety inside vehicles.
A body in white is composed of different grades of steel and their position depends on their functions. In some parts, it may be necessary to join three dissimilar sheets by resistance spot welding (RSW), one very thin with two thicker. These combinations create very dissymmetric assemblies that raise problems of weldability with difficulties to grip the thin sheet with the others, as mentioned by Nielsen [1] or Kaars [2]. In this study, the focus is on a dissymetric assembly made with a low-carbon galvanized steel sheet (AM54 - 0.57 mm deep), a galvanized high-strength steel sheet (DP600 - 1.47 mm deep) and a press hardened steel sheet coated with aluminium-silicon (Al-Si) (Usibor - 1.2 mm deep).
The purpose of this study is to understand the source of the difficulties encountered during the RSW of this assembly. The aim is to identify the parameters that influence the formation and development of the nugget and its penetration into the thin sheet.
This study is carried out by a numerical approach using the Forge® software. Particular attention is paid to interfacial phenomena.
First, the validation of the model is done by comparing the numerical and experimental results obtained during welding tests [3]. Then, it is used here mainly to highlight the main mechanisms that influence the formation and development of the nugget within the dissymetric assembly.

2 Material and methods

The welding parameters imposed are electric current (I=8500 A), load (F=4000 N) and welding time (t=350 ms). To reveal the growth of the molten pool in the dissymmetric assembly, interrupted welding tests are performed in the range [80 - 350] milliseconds. The voltage between the two electrodes is recorded at a frequency of 1 kHz with a SEFRAM digital recorder (DAS1400). The experimental contact radii at the two electrode/sheet interfaces are first measured at the end of the clamping step with Prescale® pressure-sensitive paper. Then, they are also measured after the cooling step, from interrupted welds, with an Altimet optical profilometer (Altisurf 500 with CM300 probe) with precision of ± 50 µm. Irreversible marks on the surface of the sheets after the electrodes were indented are assumed to be circular. The experimental value of the final thickness (eA) of the assembly (2.75 ± 0.05 mm) is measured from the macrograph corresponding to the total welding time (350 ms). The main dimensions of the nugget (overall thickness (eN), radius at the S1/S2 interface (rN1), radius at the S2/S3 interface (rN2), penetration into the thin sheet (p)) are measured from the macrographs at different interrupted times by the ImageJ® software. Accuracy is related to pixel size (± 50 µm).

3 Numerical Model

3.1 Geometry

When creating the numerical model, the geometry of the model can be assumed to be 2D axisymmetric due to the revolution geometry of the electrodes (Figure 1). The CuCrZr electrodes used (ISO 5821-A0-13-18-18-32) have a diameter of 13 mm and a bending radius of 32 mm.
The sheets (AM54, DP600, Usibor®) are considered without their coating in the model, and have respectively a thickness of e1 = 0.55 mm, e2 = 1.45 mm and e3 = 1.14 mm. Thermal and electrical resistances of the coatings are taken into account by the interfacial properties under contact conditions (section 3.5).

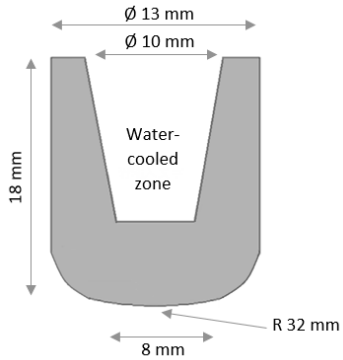

Figure 1. Reference electrodes type A0-13-18-32 – diameter 13mm, curvature radius 32mm

3.2 Mesh

The initial mesh size of the assembly (Figure 2) uses linear triangular elements. The size of an element is defined by the average length of its edges. Depending on the location of the assembly, the size of the elements are not the same, the mesh is refined near the contact zones and coarsened farther. Indeed, at the level of the contact areas, the average size of the elements is 0.1 mm. In areas where the variation of physical phenomena and gradients must be high, the average size is 0.25 mm. In the other least affected areas, the average size of the 0.4 mm.

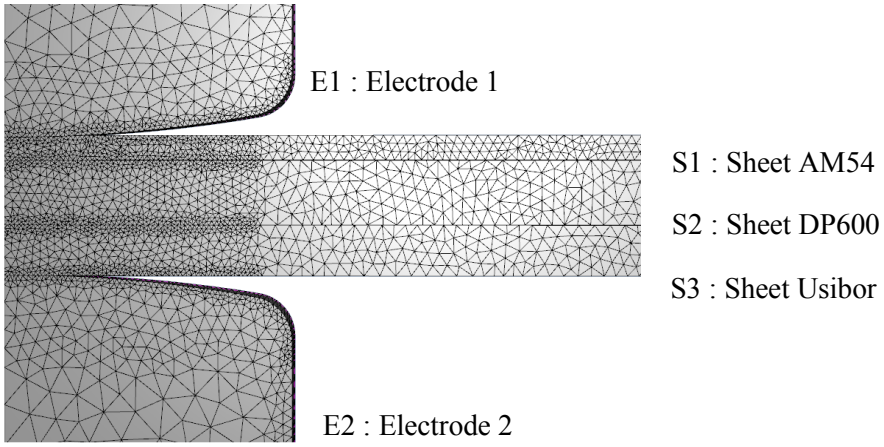

Figure 2. Initial mesh of the assembly

The trigger criterion of the remeshing is automatic and is based on the increase in maximum deformation between two remeshing operations. The remeshing is triggered after a maximum deformation increase of 100%. The advantage of this criterion is that it depends on the time step and on the deformation rate.

3.3 Governing equations

According to similar recent numerical works ([4], [5], [6]), the model developed here takes into account the main phenomena involved in the process (electric, thermic, mechanic) with their coupling occurring inside the material and at the interfaces. The metallurgical phase transformations in the steels are not explicitly taken into consideration in this model, but their main effect concern, principally, the residual stresses [7], which are not in the focus of this study. The effect of the magneto-hydro-dynamic (MHD) phenomenon that are susceptible to occur inside the molten nugget are supposed negligible and are not taken into consideration, according to Wan [6], Wang [5], or Raoelison [4], but in contradiction with Wei ([8], [9]) or Li [10]. The equations of the model are not detailed here.

3.4 Boundary conditions

During the various steps (clamping, welding and forging), specific boundary conditions are applied (Figure 3):

- While clamping, welding and forging steps, a mechanical load of 4000 N is applied to the upper electrode.
- For welding step, the electrical current of 8500 A is applied to the upper electrode, and a mass V = 0 to the lower electrode.
- During welding and forging steps, water convection exchanges are imposed inside the electrodes in order to cool them, and radiative and convective air exchanges are imposed on the surfaces of the sheets and electrodes.

The parameters used in the numerical simulation are the same as those used in the experimental tests [3].

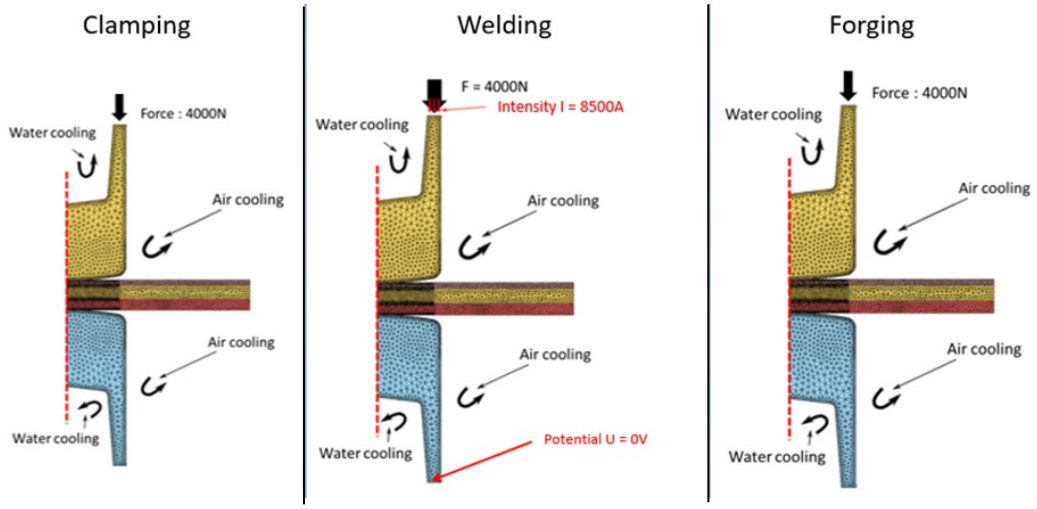

Figure 3. Boundary conditions applied on the model corresponding to the welding conditions

Due to the curved radii of the electrodes, their tips indent in the sheets during the welding process. In addition, a significant thermal expansion of the sheets occurs due to the high temperature reached inside the assembly. As a result, contact conditions change at the macroscopic scale.

Indeed, the apparent electrode/sheet (E/S) contact surface increases during the welding time, and the current density in the assembly and the contact pressure at the interfaces decrease accordingly. For mechanical contact modeling, sliding conditions are assumed for the (E/S) and sheet/sheet (S/S) interfaces.

When contact surfaces are analyzed at the microscopic scale, imperfections in the contact surfaces (surface roughness, chemical pollutants) cause the interfaces to be less than perfect and a contact resistance to current and heat flow is present. The electrical and thermal resistances of the E/S and S/S interfaces are taken into account by 3 contact parameters (ECR, TCR,) [11]. The electrothermal contact conditions are considered to be purely resistive. The energy production by Joule effect ϕ inside the ECR, crossed by the current density J, (ϕ= ECR.J² (W/m²)), is distributed on the two surfaces in contact, thanks to a partition coefficient (α) imposed at 0.5 ([12], [13]).

3.5 Materials and contacts data

Strong differences exist between physical and mechanical properties of the sheets (Table 1), (Figure 4). During the welding, the temperatures inside the sheets vary in a large range of temperature, from the ambient temperature to high temperatures higher than the liquidus temperature (1535°C). To calculate the strains, a good description of the behaviors of the material at high temperature is needed [7]. Near the melting temperature,

sheets become sensitive to the strain rate. The description of the viscoplastic behavior of steels has been input in data tables. The work-hardening curves at different strain rates from 10^{-3} to 10^{+3} s^{-1} and at different temperatures from 20 °C to 1600 °C are given for each steel. The material data for the sheets are given by the software JMatPro® which allows the calculation of the thermophysical and mechanical properties of the steels from their chemical composition. For CuCrZr alloy, plastic behavior has been assumed [14].

Table 1. Thermo-physical and mechanical properties of the sheets at ambient temperature (293 K)

	Thermo-physical properties at 293 K				Melting temperature	Mechanical properties at 293K	
Name	**Density [kg.m^{-3}]**	**Heat capacity [J.kg^{-1}.K^{-1}]**	**Thermal conductivity [W.m^{-1}.K^{-1}]**	**Electrical resistivity [µΩ.m]**	**$T_{solidus}$ [°C]**	**Re [MPa]**	**Rm [MPa]**
AM54	7750	446	66.1	0.12	1531	180	315
DP600	7790	447	42.2	0.27	1480	383	626
Usibor®	7940	452	38.6	0.24	1456	1100	1500

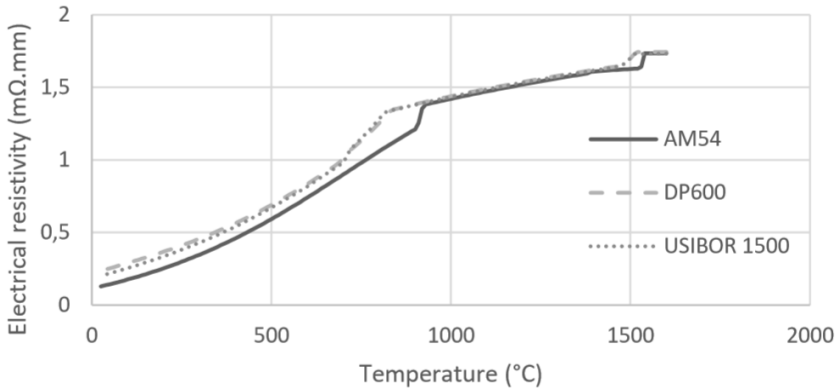

Figure 4. *Electrical resistivity evolutions versus temperature of the steel sheets [3]*

In several RSW numerical models [9], [5], [15], the contact resistances are calculated by correlations or phenomenological laws and the TCR are derived from the ECR using the Wiedmann-Franz law. While in this study, concerning the interfacial properties of the E/S and S/S contacts, the evolutions of the thermal and electrical contact resistances, TCR and ECR, were characterized on a specific device [16] as a function of pressure and temperature (Figure 5, Figure 6). Due to the plastic deformations of the asperities, the evolutions of the ECR and TCR are irreversible as a function of pressure and temperature. The bulk resistances of the coatings are included into the contact resistance values. Due to the specific properties of the Al-Si coating (conductivity, hardness and roughness [16], [3] lower) compared to the zinc coating, the contact resistances (ECR (S2/S3), ECR (S3/E2)) of both interfaces with the Usibor® plate are higher (Figure 5, Figure 6). In this study, contact resistances are implemented in the numerical model but their irreversibility as a function of temperature and pressure is not yet taken into consideration.

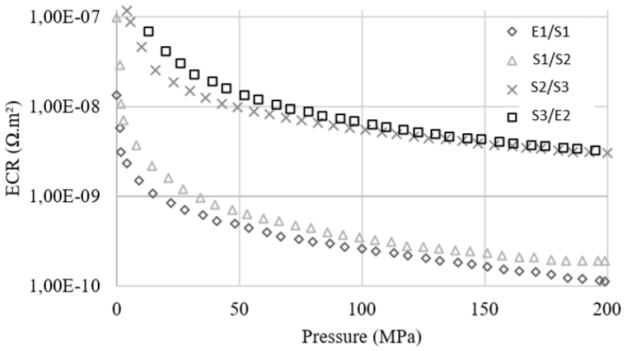

Figure 5. Experimental evolution of the ECR for each interface versus the contact pressure P at ambient temperature

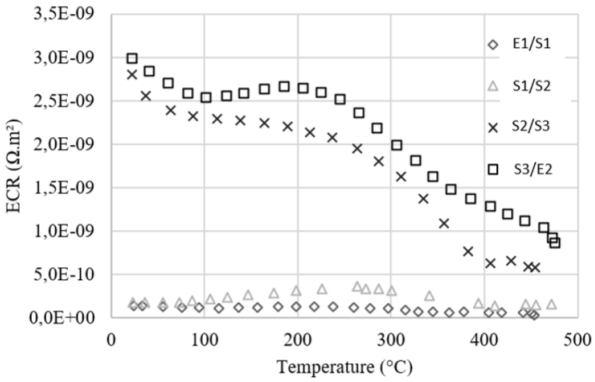

Figure 6. Experimental evolution of the ECR for each interface versus the temperature at 200 MPa

4 Results and analysis

4.1 Voltage between the electrodes

The evolutions of the numerical and experimental upper electrode voltage are really in good accordance until 40 ms (Figure 7). Just after 40 ms the numerical curves present a jump of the potential not observed experimentally. After 150 ms the numerical and experimental curves are in good accordance again.

The voltage depends on the electric current evolution imposed (Figure 7) and on the dynamic electrical resistance of the assembly which varies with the electrical contact resistances, the electrical resistivity of the sheets, the thickness of the sheets, and with the contact radii. The pic of tension is obtained after that the welding intensity reaches its maximal value on the plateau (Figure 7).

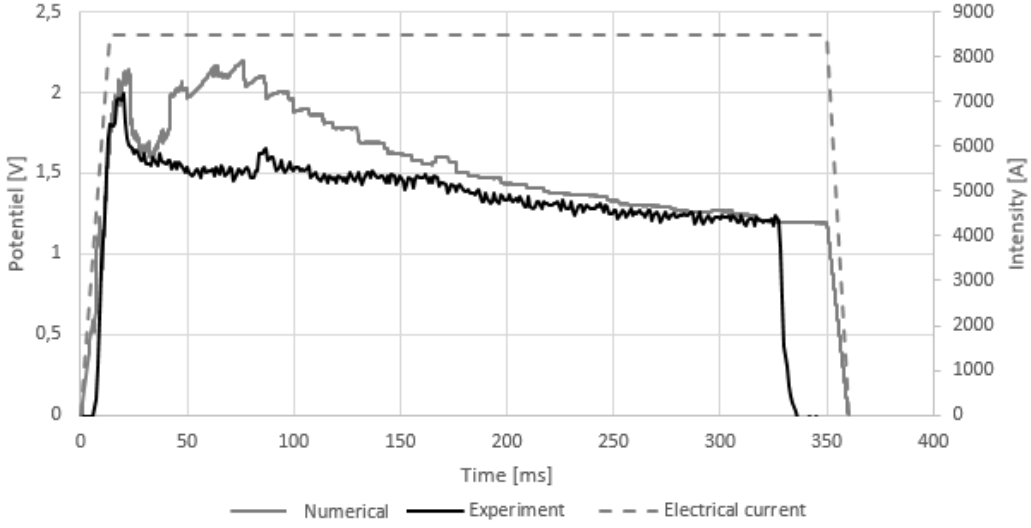

Figure 7. Numerical and experimental voltage evolution and electrical current profile

4.2 Strains of the assembly, contact radii and thickness

At the end of the clamping stage, the experimental contact radii measured with pressure-sensitive paper Prescale® appear higher than the numerical values (Figure 8). The measurement technique with ink-laden microbeads may overestimate the values of the radii [3] and could explain the observed discrepancies. During the welding stage, at the electrode/thin sheet interface (E1/S1), the evolution of the measured and calculated radii intersects around 80ms, then diverge after (Figure 8). The numerical radii calculated are higher than the experimental radii measured. For the interface Usibor/electrode (E2/S3), the calculated values of the contact radii are lower than the experimental ones on the whole welding time (Figure 8). Despite the differences, the dynamic of the evolutions of the E/S contact radii obtained by the numerical model are rather similar to values issue from experimental tests.

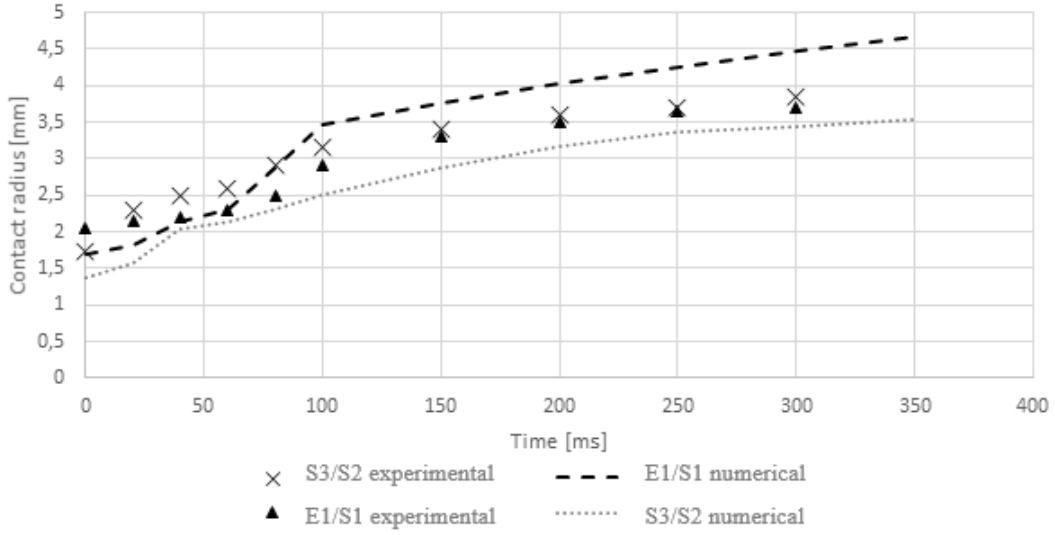

Figure 8. Comparison between numerical and experimental contact radii evolutions for the two E/S interfaces

The assembly of three sheets also meets a variation of its thickness eA (eA=e1+e2+e3) during the process. Two antagonist forces are responsible of this variation:

- The squeezing force applied by the electrodes which induces the indentation of the rounded tip electrodes inside the sheets
- The thermal dilatation of the materials

The thickness increases during the first period of the welding step (0 to 190 ms) (Figure 9), due to the important temperature rise in the assembly. During this period of time the heat production by Joule effect is largely higher than the thermal losses, because of the electrical contact resistance effects and because of the small contact areas which induce high current density values in the assembly. The indentation of the electrode tips inside the sheets begins, but the evolution of the thickness is mostly driven by the thermal

dilatation. The molten pool size also increases quickly in thickness until around 200 ms (Figure 13).

For a time greater than 190 ms the thickness of the assembly decreases. Indentation of electrode tips inside the sheets become the prevalent factor, due to the softening of the sheets with the strong heating in the first moment.

When the welding current is interrupted after 350 ms, the thickness decreases continuously, mainly due to the thermal shrinkage, during the forging stage till 860 ms and during the air cooling stage (duration of the cooling stage : 120s).

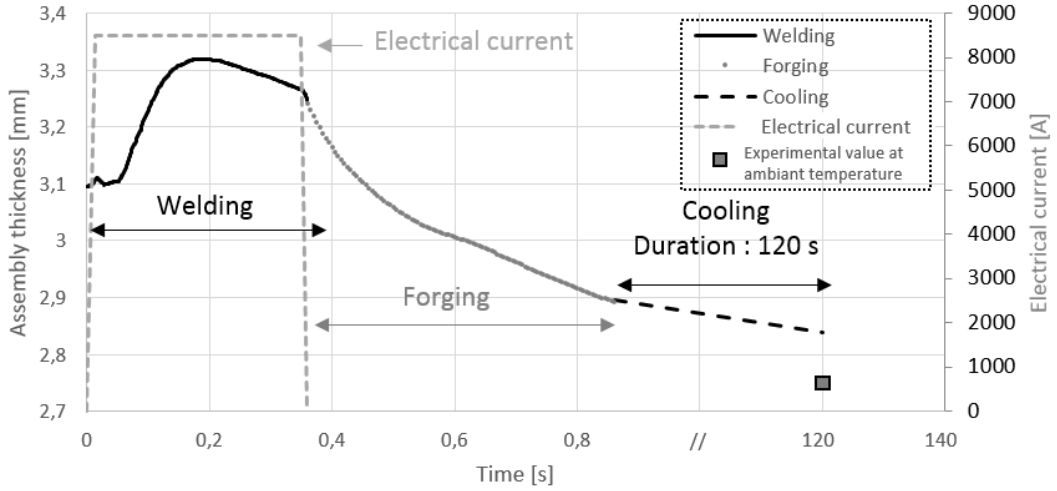

Figure 9. Evolution of the assembly thickness

4.3 Radius and thickness of the molten pool, penetration in the thin sheet

The numerical shapes of the molten pool appear in good accordance with experimental ones for different interrupted times (80, 150, 300 ms) (Figure 10). However, the sizes cannot be compared directly. The numerical molten pool sizes are obtained when the fusion zone meets high temperatures (2800-3000 °C) and high dilatation rate. In the second case, the experimental solidified nugget is obtained after thermal shrinkage at ambient temperature. Only the experimental and numerical localization and dynamic evolution of the nugget can be compared.

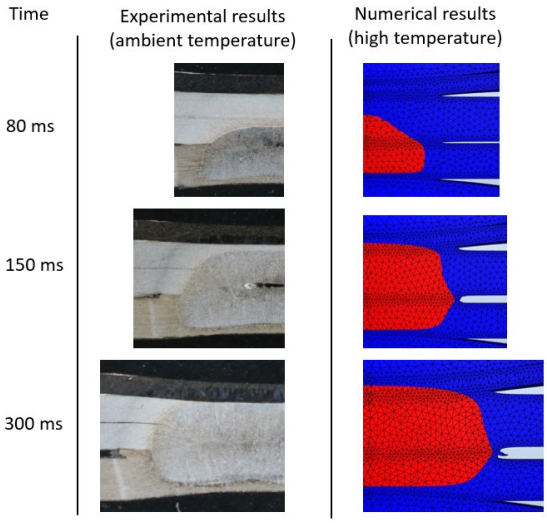

Figure 10. Comparison of the localization and the shape of the numerical molten pool (high temperature) and the experimental nugget (ambient temperature)

The calculations show that the molten nugget appears inside the Usibor plate around 40 ms (Figure 11) at the opposite of the thin sheet. After it develops quickly in thickness inside the DP600 and towards the AM54 thin sheet (Figure 11). The origin is linked to the huge contact resistances at interfaces with the Usibor sheet which initiate overheating at these interfaces and locate the hot spot within the Usibor sheet.

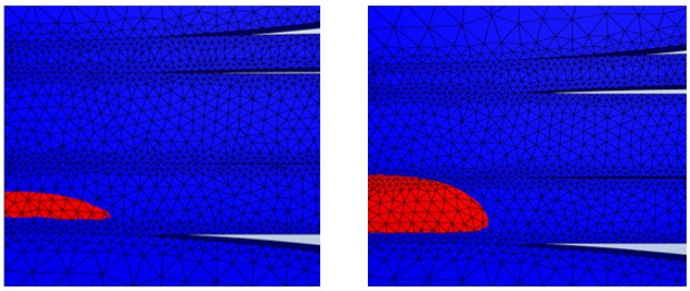

Figure 11. Localization and shape of the molten pool at 40ms and 60ms

In this section, the numerical and experimental dimensions of the nugget are compared more precisely (thickness eN, radii (rN1 rN2), penetration in the thin sheet p) (Figure 12).

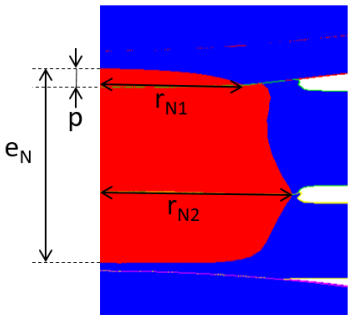

Figure 12. Dimensions of the nugget: eN (thickness), rN1 (radius at the interface S1/S2), rN2 (radius at the interface S2/S3), p (penetration inside the thin sheet)

The numerical and experimental evolutions of the thickness of the molten pool present similar dynamics (Figure 13). The thickness increases quickly, then meets a maximum around 200 ms, and decreases slowly until the electrical current is cut off at the end of the welding at 350 ms. The numerical values, taking into account the strong thermal dilatation of the molten pool, are logically higher than the experimental values measured at ambient temperature after cooling of the assembly. The numerical thickness values obtained after forging stage from 3 interrupted points (80, 150, 300 ms) are logically nearer (Figure 13).

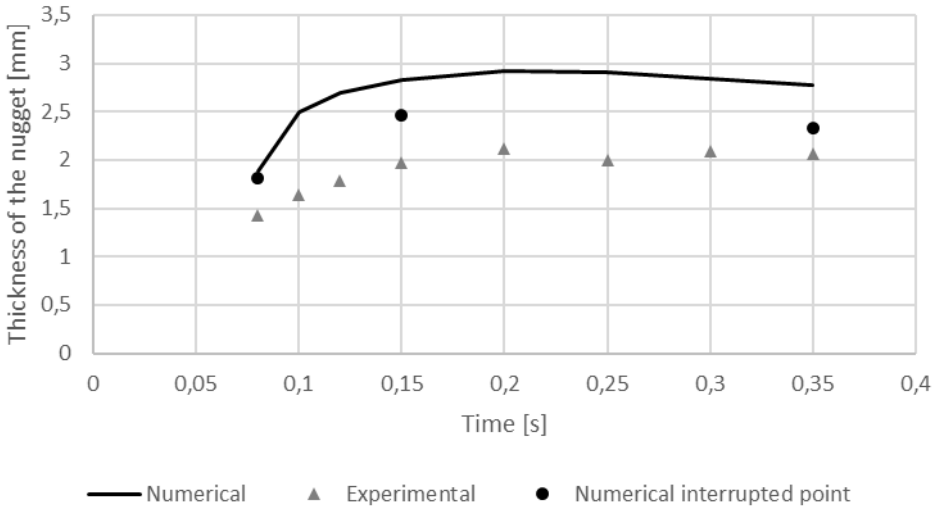

Figure 13. Evolution of the depth of the molten pool (during the welding) and the nugget (after cooling)

The thickness evolution of the molten pool is driven by the equilibrium between the heating by Joule effect, at the interfaces (ECR.J^2 (W/m^2)) and inside the sheets ($1/\sigma.J^2$ (W/m^3)), and the heat losses mainly by conduction through the electrodes. Indeed, until the values of the contact radii (Figure 8) remain sufficiently low, heating is dominant and the nugget thickness increases quickly. After 200 ms when the contact radii reach high values with the indentation of the electrode tips inside the sheets, the current density drops causing a decrease of the power heating and the heat losses increase and become prevalent. Consequently, the nugget thickness regresses slightly.

Furthermore, the evolutions of the numerical and experimental nugget rN2 are in pretty good adequacy (Figure 14), by taken into consideration the preceding remarks on the potential causes of distortions.

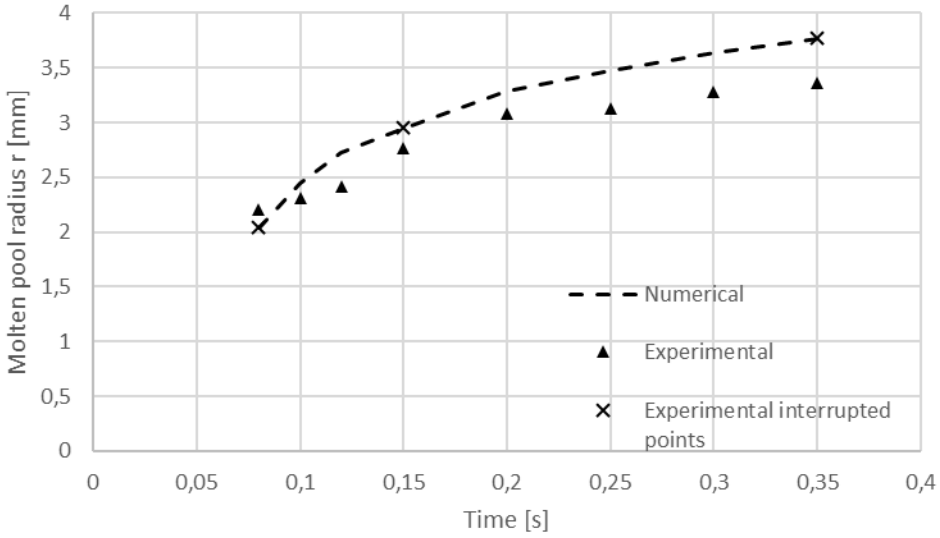

Figure 14. Comparison between experimental nugget radius and numerical molten pool radius during welding stage

The penetration of the molten pool inside the AM sheet reaches a maximal value 0.34 mm at 200 ms (Figure 15) and decreases slightly after. The experimental value 0.14 mm measured after the end of the cooling stage is significantly lower, which indicates that the numerical molten pool thickness is certainly overestimated. The radius rN1 of the molten pool at the contact E1/S1 increases continuously during the welding stage and reaches 3 mm.

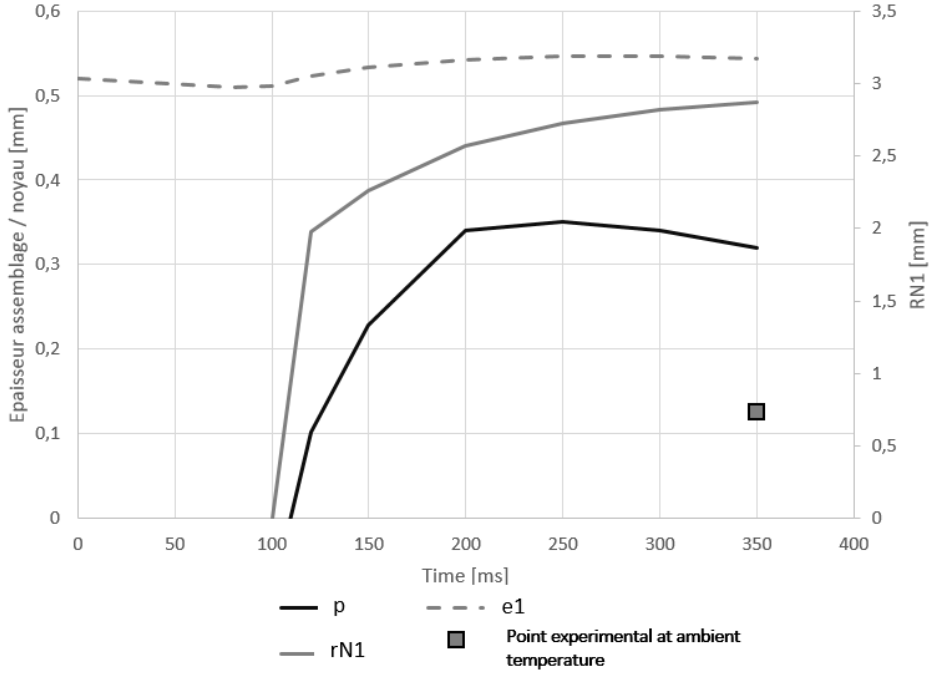

Figure 15. Penetration of the molten pool inside the AM sheet

5 Conclusion

In this study, achieved in partnership with ArcelorMittal, a numerical model has been developed using the software Forge® to simulate the resistance spot welding of a 3 dissimilar sheets assembly, including a very thin sheet. The aim is to give a better understanding of the difficulties encountered to succeed the weldability of the thin sheet. The good adequacy found between numerical and experimental results, concerning the E/S contact radii, the size of the nugget with the penetration inside the thin sheet and the voltage between electrodes, proves the reliability of the model and the suitability of the software Forge® to simulate the RSW process. The huge electrical and thermal contact resistances at the two interfaces with the Usibor sheet, because of the Al-Si coating, promote the initiation of the nugget inside this sheet, far from the thin sheet. The growing of the nugget in thickness and the penetration inside the thin sheet appear in the first moment of the welding stage, till the contact radii become too important due to indentation of rounded tip electrodes inside the sheets. After the nugget progresses only in diameter at the two S/S interfaces till the end of welding stage. Despite these good tendencies given by the model an abnormal overheating is observed numerically in the assembly.

To improve the numerical model, a great attention should be paid to the modelling of the contact conditions. Irreversibility laws for the contact resistances should be imbedded and optimization of the physical properties of the molten pool could be assessed, in particular an equivalent thermal conductivity to take into account the convective phenomena.

Acknowledgement

The authors would like to thank the ArcelorMittal Global R&D for the steels supplying and the financial and technical support. The authors also would like to thank the Transvalor Company for advises and technical support.

References

[1] C. V. Nielsen, K. S. Friis, W. Zhang, N. Bay, ‘Three-Sheet Spot Welding of Advanced HighStrength Steels’, Welding Journal 90, pp. 32s-40s, 2011.

[2] J. Kaars, P. Mayr, K. Koppe, ‘Simple transition resistance model for spot welding simulation of aluminized AHSS’, Math. Model. Weld Phenom 11, pp. 32s-40s, 2016.

[3] E. Geslain, Soudage par résistance des tôles fines revêtues : formation du noyau dans un assemblage de trois tôles, thesis, Université de Bretagne Sud, 2018.

[4] R. Raoelison, A. Fuentes, C. Pouvreau, P. Rogeon, P. Carre, F. Dechalotte, ‘Modeling and numerical simulation of the resistance spot welding of zinc coated steel sheets using rounded tip electrode: analysis of required conditions’, Appl. Math. Model 38, pp. 2505-2521, 2014.

[5] J. Wang, H. P. Wang, F. Lu, B. E. Carlson, D. R. Sigler, 'Analysis of Al-steel resistance spot welding process by developing a fully coupled multi-physics simulation model', International Journal of Heat and Mass Transfer 89, pp. 1061–1072, 2015.
[6] Zixuan Wan, Hui-Ping Wang, Min Wang, Blair E. Carlson, David R. Sigler, 'Numerical simulation of resistance spot welding of Al to zinc-coated steel with improved representation of contact interactions', International Journal of Heat and Mass Transfer 101, pp. 749–763, 2016.
[7] J.M. Bergheau, 'Modélisation numérique des procédés de soudage', Techniques de l'ingénieur, 2004.
[8] P.S. Wei, S.C. Wang, M.S. Lin, 'Transport phenomena during resistance spot welding', J. Heat Transfer 118, pp. 762–773, 1996.
[9] P.S. Wei, T.H. Wu, 'Electrical contact resistance effect on resistance spot welding', International Journal of Heat and Mass Transfer 55, pp. 3316-3324, 2012.
[10] Y. Li, Z. Luo, Y. Bai, S. S. Ao, 'Investigation of induced magnetic force on liquid nugget during resistance spot welding', Sci. Technol. Weld. Join. 18-4, pp. 329–336, 2013.
[11] G. Sibilia, Modélisation du soudage par point: Influence des conditions interfaciales sur le procédé, thesis, Ecole Polytechnique de l'Université de Nantes, 2003.
[12] G. Le Meur, G. Bourouga and B. Bardon, 'Microscopic analysis of interfacial electrothermal phenomena – Definition of a heat generation factor', International Journal of Heat and Mass Transfer 49, pp. 387-401, 2006.
[13] P. Rogeon, R. N. Raoelison, P. Carre And F. Dechalotte, 'A Microscopic Approach to Determine Electrothermal Contact Conditions During Resistance Spot Welding Process', J. Heat Transfer, vol 131, pp. 022101-1 – 022101-11, 2009.
[14] E. Gauthier, Etude expérimentale et numérique de la dégradation cyclique des électrodes en CuCrZr lors du soudage par résistance par point, thesis, Université de Bretagne Sud, 2014.
[15] S. Babu, M. Santella, Z. Feng, B. Riemer, J. Cohron, 'Empirical model of effects of pressure and temperature on electrical contact resistance of metals', Sci. Technol. Weld. Joining 6 (3), pp. 126–132, 2001.
[16] E. Geslain, P. Rogeon, T. Pierre, C. Pouvreau And L. Cretteur, 'Coating effects on contact conditions in resistance spot weldability', Journal of Materials Processing Tech. 253, pp. 160167, 2018.

Table

Tables